

Spider-Like Oligothiophenes

Tiziana Benincori,^[b] Marcello Capaccio,^[c] Filippo De Angelis,^[d] Luigi Falciola,^[e] Michele Muccini,^[f] Patrizia Mussini,^[e] Alessandro Ponti,^[g] Stefano Toffanin,^[f] Pietro Traldi,^[h] and Francesco Sannicolò*^[a]

Dedicated to Professor Renato Ugo, enthusiastic supporter of this work

Abstract: Careful analysis and comparison of optical and electrochemical data available in recent literature for multi-thiophene molecular assemblies suggested a few basic rules for the design of structurally simple and easily accessible oligothiophenes endowed with properties not far from those exhibited by much more complex and synthetically demanding architectures. The synthesis and computational investigation of three examples of a class of oligothiophenes (spider-like) tailored according to these indications are reported together with their exhaustive optical and electrochemical characterization. The new compounds (**T9**₅, **T14**₆, **T19**₇) are characterized by a thiophene,

a 2,2'-bithiophene and a 2,2',5',2''-terthiophene unit (the spider body) fully substituted with 5-(2,2'-bithiophenyl) pendants (the spider legs). Absorption and electrochemical data are in good agreement and point to a high π -conjugation level, comparable to those displayed by much larger assemblies. Electrode potential cycling in proximity of the first oxidation peak affords fast and reproducible formation of conducting, highly stable $[\text{TX}_n]_m$ films,

Keywords: conducting materials • dendrimers • electrochemistry • oligothiophenes • UV/Vis spectroscopy

mainly consisting of dimers ($m=2$). Electrooxidation kinetic experiments on deuterium-labelled **T9**₅, coupled to laser-desorption-ionization mass spectroscopy on the resulting dimer demonstrated that the coupling process is extremely regioselective in the α positions of the more conjugated pentathiophene chain. The optical and the electrochemical properties of the films are reported and discussed. A peculiar feature is their impressive charge-trapping ability. Spider-like oligothiophenes are promising materials for applications as active layers in multifunctional organic devices.

Introduction

A recent trend in designing materials for optoelectronic applications focuses on multi-thiophene molecules character-

ized by the overall number of thiophene units, by the nature of the substituents on them, inter-ring connectivity, molecular symmetry and shape. Swivel-cruciform,^[1] star-^[2] and X-shaped,^[3] and dendrimeric oligothiophenes^[4,5] have been

[a] Prof. F. Sannicolò
Dipartimento di Chimica Organica e Industriale
C.I.MA.I.NA, Università di Milano, ISTM, CNR, via Venezian 21
20133 Milano (Italy)
Fax: (+39)02-5031-4139
E-mail: francesco.sannicolò@unimi.it

[b] Prof. T. Benincori
Dipartimento di Scienze Chimiche ed Ambientali
Università dell'Insubria, via Valleggio 11
22100 Como (Italy)

[c] Dr. M. Capaccio
C.I.MA.I.NA., Università di Milano, via Celoria 16
20133 Milano (Italy)


[d] Dr. F. De Angelis
ISTM-CNR, Via Elce di Sotto 8
06123 Perugia (Italy)

[e] Dr. L. Falciola, Prof. P. Mussini
Dipartimento di Chimica Fisica ed Elettrochimica
C.I.MA.I.NA, Università di Milano, via Golgi 19
20133 Milano (Italy)

[f] Dr. M. Muccini, Dr. S. Toffanin
ISMN—Istituto per lo Studio dei Materiali Nanostrutturati-CNR,
Via P.Gobetti, 101
40129 Bologna (Italy)

[g] Dr. A. Ponti
ISTM—Istituto di Scienze e Tecnologie Molecolari-CNR
via Golgi 19, 20133 Milano (Italy)

[h] Dr. P. Traldi
ISTM—Istituto di Scienze e Tecnologie Molecolari-CNR
Dipartimento di Scienze Chimiche
Università degli Studi di Padova, Via Marzolo 1
35131 Padova (Italy)

 Supporting information for this article is available on the WWW under <http://www.chemeurj.org/> or from the author.

prepared in the last few years and, in some cases, preliminary practical applications of these compounds as sensitive materials for OFETs and photovoltaic devices have been described.

The world record of regioregularly assembled thiophene units belongs to Bäuerle and co-workers who very recently published a molecule consisting of 90 thiophene rings,^[4] breaking Advincula's previous score which was "only" 30.^[5a,b]

The synthetic effort required to synthesize such complex molecular architectures is understandably high, due to the considerable number of steps necessary to progressively increase the molecular size starting from small units, even though the experimental methodologies employed are often reported as high-yield procedures. Apart from the aesthetic appeal exerted by these large and constitutionally ordered molecules, the question is whether the game is worth the candle in terms of synthetic feasibility and properties. To answer this question it would be important to compare the basic properties of these sophisticated molecules with those exhibited by the linear α -oligothiophenes chosen as reference substrates. This is, however, a difficult task, since only selected parameters are reported in literature for the different classes of compounds, which prevents a complete and reliable comparison between all of them.

The situation is further complicated by the fact that some key parameters are often evaluated not only under different experimental conditions (solvent, concentration, reference electrode), but also by unstandardized procedures. For example, in optical absorption experiments sometimes the maximum and sometimes the onset of the curve are reported; in electrochemical measurements either the formal potentials (E^0), or the peak potentials (E_p), or the onset potentials (E_p^*) are indiscriminately used for both oxidation and reduction. Some normalization is possible, instead, for spectroscopic data, in spite of several difficulties. Thus, we have been able to collect from the literature the optical band-gaps calculated from the λ_{\max} , $E_g(\lambda)$ (Figure 1a, b), and from the λ_{onset} values, $E_g^*(\lambda)$ (Figure 1c), for α -linear (\mathbf{T}_n)^[6] and for some classes of branched oligothiophenes (Scheme 1) as a function of the reciprocal of the overall number of thiophene units (n) or of the number of thiophene units in the longest α -conjugated chain present in the molecule (n_α). Both n and n_α are reported for each compound in Scheme 1, together with the number of the synthetic steps required for its preparation and the overall yield (%) starting from commercially available "inexpensive" compounds (less than 12 USD per gram).

It is evident that the molecules reported in Scheme 1 are only selected examples of the much more ample and continuously growing family of the multi-thiophene molecular assemblies.^[7] In any case, the data reported in Figure 1a–c give several interesting indications. Figure 1a shows that the $E_g(\lambda)$ values calculated from λ_{\max} for all of the multi-thiophene molecules reported in Scheme 1 are much higher than those found for linear α -oligothiophenes consisting of the same number of heterocyclic units. This is expected if

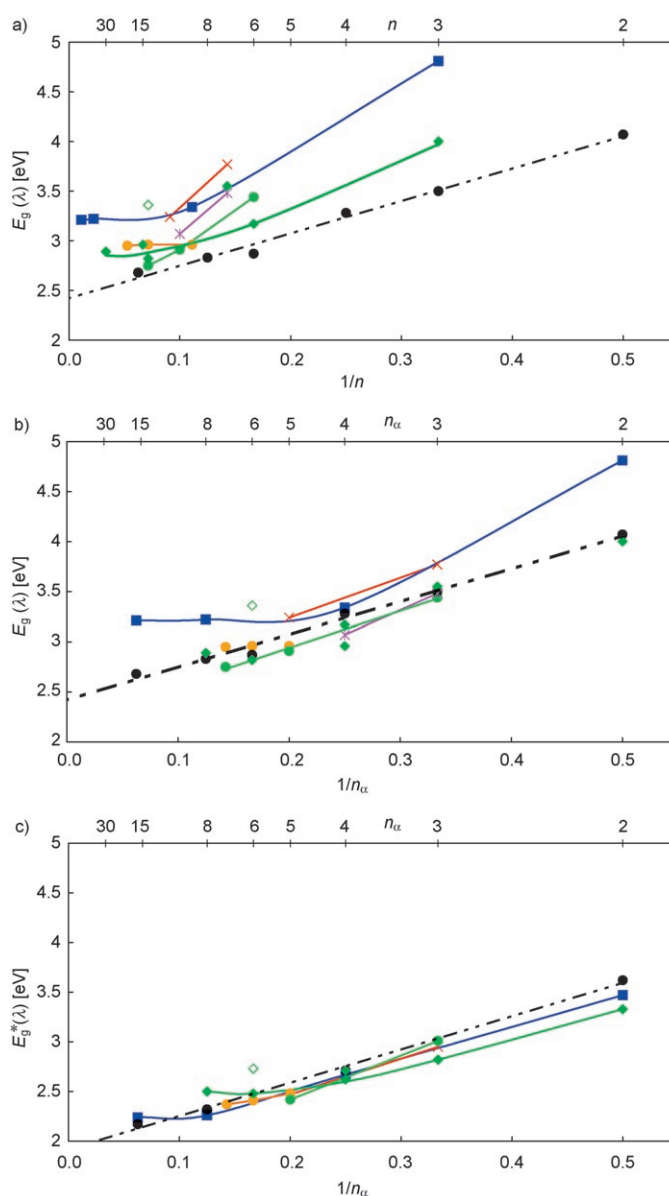
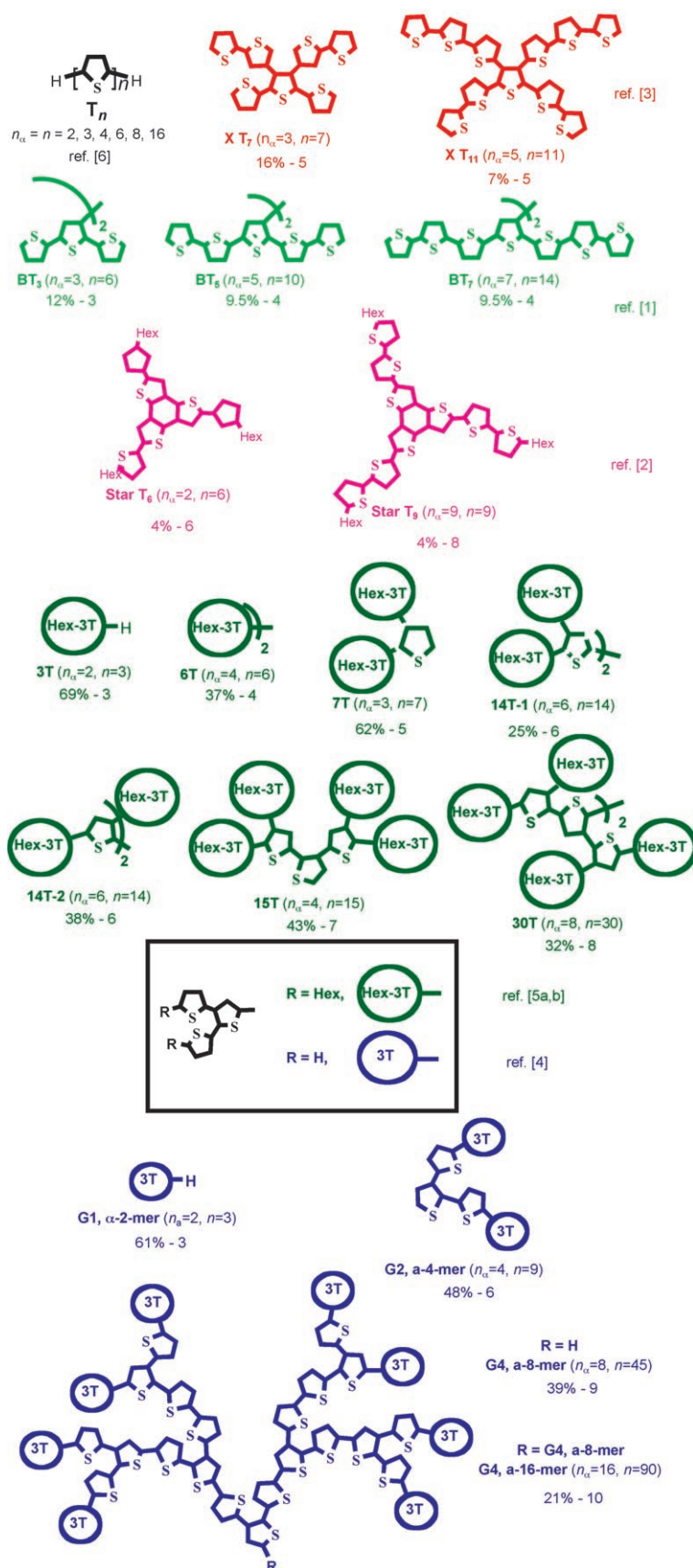


Figure 1. Optical band-gaps for the compounds reported in Scheme 1: a) $E_g(\lambda)$ calculated from λ_{\max} and plotted as a function of the reciprocal of the overall number of thiophene units n ; b) $E_g(\lambda)$ calculated from λ_{\max} and plotted as a function of the reciprocal of the number of thiophene units in the longest α -conjugated chain, n_α ; c) $E_g^*(\lambda)$ calculated from λ_{onset} and plotted as a function of $1/n_\alpha$. Different colors refer to different families of literature compounds in Scheme 1; the empty green diamond corresponds to Advincula's **14 T-2**. Yellow circles refer to the **TX_n** compounds described in this paper (Scheme 2).

considering that all the rings are conjugatively interconnected in linear α -oligothiophenes, while shorter α -conjugated sequences are present in all the other systems. It is also worth noting that the $E_g(\lambda)$ values progressively decrease as n increases up to the critical value of 8–9. This trend flattens for higher n values, and, in Advincula's series, dendrimers with 15 and 30 thiophene units display very similar $E_g(\lambda)$ values (2.9 and 2.95 eV), and the same observation works for Bäuerle's **G2,a-4-mer** ($n=9$), **G4,a-8-mer** ($n=45$) and



Scheme 1. Classification of linear and branched oligothiophenes. The acronyms defined by the authors are used when available. Specific colors group substrates of the same class and refer to the colors in Figure 1a–c. Overall preparation yields [%] and the numbers of the synthetic steps are reported for each compound.

G4,a-16-mer ($n=90$) for which very similar $E_g(\lambda)$ values were found (3.34, 3.22 and 3.21 eV, respectively).

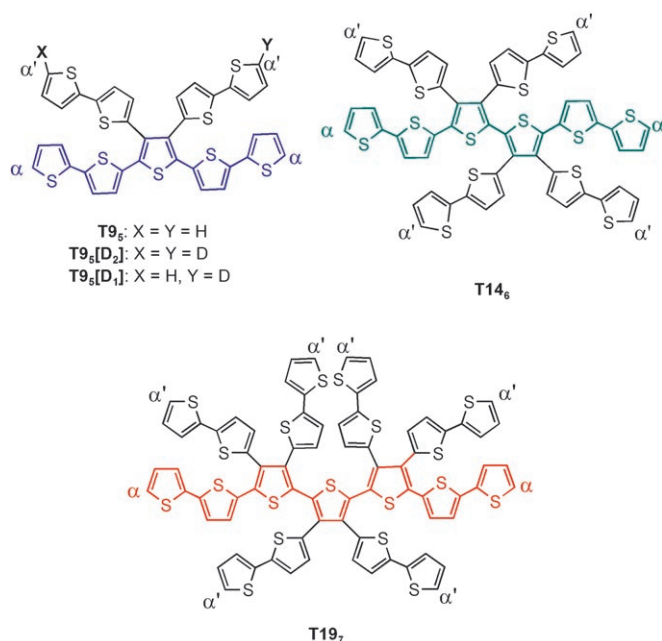
The data reported in Figure 1b demonstrate the strong relationship existing between the $E_g(\lambda)$ values calculated from the λ_{\max} and n_α . The following “rule” can be deduced: even big dendritic molecules having many α -conjugated branches with different lengths display an optical gap close to that exhibited by the unsubstituted α -oligothiophene T_n with n corresponding to the longest α -conjugated branch of the dendrimer. Large multi-thiophene molecules display, however, energy gaps generally higher than expected due to some distortion from coplanarity of the main α -conjugated chain produced by branching. This behavior is evident in the highest terms of Bäuerle’s series and striking in Advincula’s **14T-2** ($n_\alpha = 6, n = 14$, empty green diamond), where the interannular torsion about the central bond, as recognized in the paper,^[5b] halves the expected gap value of the T_6 to that of the T_3 .

It is understandable, however, that the electronic spectra of very large molecular assemblies would be better described by λ_{onset} than by λ_{\max} , since absorption curves undergo massive broadening as the molecules become larger and larger. Plotting the energy gap values calculated from λ_{onset} , $E_g^*(\lambda)$ against $1/n_\alpha$ gives a striking demonstration of the close relationship between these parameters. There is a remarkable crowding of data along the line representing the properties of the T_n . It is interesting to note that the energy gap values substantially flatten when five α -conjugated thiophene units are present ($n_\alpha \approx 5$), independently of the total number of thio-

phene units constituting the molecule (n) and of the inter-ring connectivity. It is worthwhile noticing that the only remarkable exception in this context, that is, **T14-2**, can be again completely normalized by plotting it as a function of $n_{\alpha}=3$ instead of $n_{\alpha}=6$.

The conclusion we draw from these observations is that the synthetic engagement required to prepare molecules consisting of a very large number of thiophene rings is not always accompanied by the acquisition of extraordinary conjugation properties, even though other very interesting physical features are acquired, like high chemical stability and solubility in non-polar organic solvents.

In this context we considered an alternative, very simple design of all-thiophene assemblies, which is a compromise between size and properties, exemplified by the three "spider-like" oligo-thiophenes **T9₅**, **T14₆** and **T19₇**, characterized by a thiophene, a 2,2'-bithiophene and a 2,2',5',2''-terthiophene unit (the spider body) fully substituted with 5-(2,2'-bithiophenyl) pendants (the spider legs) (Scheme 2). In the abbreviations **TX_n**, **T** means thiophene, **X** denotes the total number of thiophene units constituting the molecule and subscript **n** the longest chain displaying exclusively α junctions.



Scheme 2. Molecular structures of **TX_n**.

Structural design was based on the following considerations:

a) All the compounds were tailored to have structural parameters (n and n_{α}) centered in the critical area discussed before, with a unique α -conjugated main chain consisting of five, six and seven thiophene units, respectively, and all the pendants belonging to much shorter α -bithiophene moieties.

- b) The **TX_n** appeared easily accessible through a single reaction (a Stille coupling reaction), mostly involving commercially available, inexpensive starting materials. Thus, the synthetic burden was much lower than that generally required to prepare any of the oligothiophenes reported in Scheme 1.
- c) The electrochemical oxidative multiplication of these substrates could generate very large all-thiophene branched macromolecules. Simple dimerization would afford materials consisting of a number of thiophene units much larger than the critical value where the electronic conjugation properties tend to flatten.
- d) Good regioselectivity could be expected in the electrochemical oxidative coupling, since, out of the many α positions of the terminal thiophene units, the two positions belonging to the main conjugated system (indicated as α in Scheme 2) should be preferred. Therefore we considered the capping of α' positions in principle unnecessary, a process which limits accessibility and multiplies the synthetic steps.
- e) The high symmetry of **T9₅** (C_{2v}), **T14₆** (C_{2h}) and **T19₇** (C_{2v}) makes the α positions of all the systems homotopic, thus a very high constitutional order could be expected in the electrooxidative coupling process.

Results and Discussion

Synthesis of TX_n: Compound **T9₅** was already known in literature.^[8] It had been obtained by reaction of bis[5-(2,2'-bithiophenyl)]acetylene with sulphur at 210 °C (57% yield). It was prepared by Stille reaction of commercially available tetrabromothiophene (**1**)^[9] with 5-tributylstannyl-2,2'-bithiophene (**2**),^[10] in the presence of [Pd(PPh₃)₄] (10% mol), in refluxing toluene (18 h, 70% yield). Column chromatography gave the product in a pure state. **T14₆** was analogously synthesized starting from hexabromo-2,2'-bithiophene (65% yield).^[11] Much more laborious was the preparation of **T19₇**. We found it very difficult to attain the substitution of all the bromine atoms of octabromo- α -terthiophene^[12] with bithienyl units. Purification required several chromatographic separations and only a small amount of pure **T19₇** was obtained, narrowing the scope of the investigation on this compound.

Complex **T9₅** and **T14₆** can be considered amongst the most accessible all-thiophene oligomers and could be prepared, if necessary, on a kiloscale level.

Solubility in organic non-polar solvents was found remarkable and in agreement with the data reported in the literature for capped and uncapped oligothiophene dendrimers.

We did not succeed in growing crystals of **TX_n** suitable for XRD analysis, which would have given important information on inter-ring torsion and hence on the electronic distribution, in particular on the most extended conjugated sequence. We resorted to DFT calculations to fill this gap.

Theoretical analysis on $T9_5$ and $T14_6$: To gain insight into the structural, electronic and optical properties of the investigated oligomers, we performed density functional theory (DFT) and time-dependent DFT (TDDFT) calculations on $T9_5$ and $T14_6$, these species allowing us to investigate the effect of increased conjugation and branching. The geometry was optimized without any symmetry constraints using the B3LYP functional^[13] and a 6-31G* basis set.^[14] On the optimized geometries we calculated the vertical absorption spectrum by TDDFT employing both the B3LYP and the PBE0 exchange-correlation functional,^[15,16] with the same 6-31G* basis set used for geometry optimization. All the calculations have been performed with the Gaussian03 program package.^[17] The optimized geometry of $T9_5$ is reported in Figure 2a along with selected geometrical parameters. A

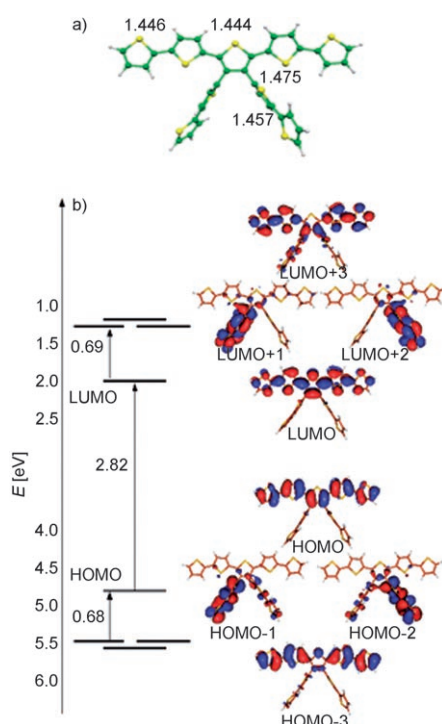


Figure 2. a) Optimized geometrical structure of $T9_5$. b) Schematic representation of the frontier molecular orbitals of $T9_5$, along with isodensity plots of selected orbitals.

schematic representation of the frontier molecular orbitals at the B3LYP/6-31G* level together with selected isodensity plots of such orbitals are reported in Figure 2b.

The optimized $T9_5$ structure shows an almost planar arrangement of the α -pentathiophene chain with two “spider legs” lying orthogonal to the “body”. The increased conjugation and charge delocalization across the α framework is reflected by the slightly shorter C–C distances interconnecting different thiophene units with respect to the sequences including α - β connections (1.446 vs 1.451–1475 Å).

For $T14_6$, we calculated two almost isoenergetic conformers, corresponding to a planar and a twisted situation with

respect to the central C–C bond (Figure 3). The twisted conformer, characterized by a twisting dihedral angle of 107.7°, is the more stable structure, being 0.5 kcal mol⁻¹ lower than

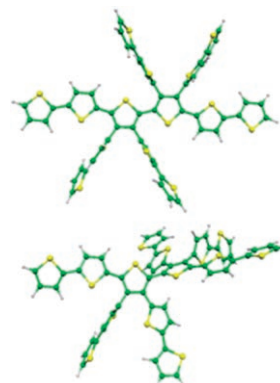


Figure 3. Optimized planar and twisted structures of $T14_6$.

the planar conformer (twisting dihedral angle of 176.6°). The small energy difference between the two conformers suggests that a high degree of conformational fluxionality effectively exists.

Inspection of the calculated electronic structure of $T9_5$ shows that the HOMO, found at -4.84 eV, is a combination of thiophene π bonding orbitals extending across the whole α -conjugated body. At lower energy (-5.52 – -5.55 eV), the HOMO–1/HOMO–2 are a degenerate couple of π -bonding orbitals confined within two spider legs, whereas the HOMO–3 (-5.61 eV), almost degenerate with the HOMO–1/HOMO–2 couple, again extends on the α framework only. The HOMO and HOMO–1/HOMO–2 have therefore a similar character although a different localization; the HOMO destabilization of ca. 0.7 eV compared to the HOMO–1/HOMO–2 couple is possibly due to the increased electrostatic repulsion arising from the proximity of five sulphur lone pairs in the former. The LUMO, calculated at -2.02 eV, is a combination of π^* orbitals extending over the α framework, followed at higher energy (-1.33 – -1.32 eV) by a degenerate couple of π^* orbitals belonging to the β branches. Almost degenerate with the LUMO+1/LUMO+2 couple, the LUMO+3 is, instead, localized on the α framework. Interestingly, the HOMO–HOMO–1 and LUMO–LUMO+1 splittings are comparable (ca. 0.7 eV).

For the more stable $T14_6$ twisted conformer we calculated a similar electronic structure as for $T9_5$, with an isolated HOMO lying at -4.92 eV and a LUMO at -1.95 eV. Notably, the planar $T14_6$ conformer shows a more positive HOMO energy than its twisted counterpart (-4.74 vs. -4.92 eV), while the LUMO energy is less sensitive to the twisting angle (-1.95 vs -2.08 eV).

Spectroscopic properties of TX_n : The UV absorption data of TX_n are reported in Figure 4 and summarized in Table 1.

The spectra of $T9_5$, $T14_6$ and $T19_7$ display multiple absorption peaks at similar energetic positions, but with different

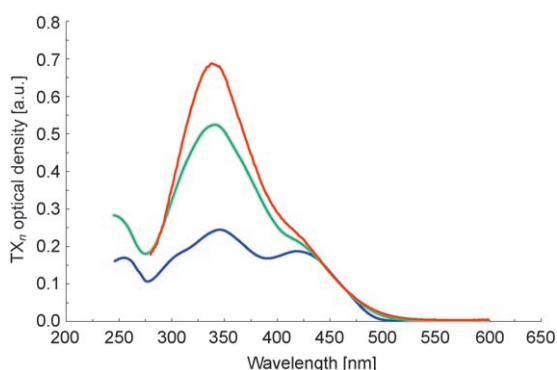


Figure 4. UV/Vis spectra of TX_n in 10^{-5}M CH_2Cl_2 solution. Color code: blue = T9_5 , green = T14_6 , red = T19_7 .

Table 1. UV/Vis absorption data (λ_{max} , λ_{onset} , ϵ) and corresponding energy gap values for TX_n in 10^{-5}M CH_2Cl_2 solution. Parenthesized extinction coefficients refer to shoulder-like signals.

TX_n	First absorption peak				Second absorption peak		
	λ_{max} [nm]	$E_g(\lambda)$ [eV]	ϵ [$\text{mol}^{-1}\text{dm}^3\text{cm}^{-1}$]	λ_{onset} [nm]	$E_g^*(\lambda)$ [eV]	λ_{max} [nm]	ϵ [$\text{mol}^{-1}\text{dm}^3\text{cm}^{-1}$]
T9_5	419	2.96	18700	500	2.48	345	24500
T14_6	420	2.96	(21300)	515	2.41	341	52500
T19_7	421	2.95	(22700)	523	2.37	338	68700

relative intensities: contrary to T14_6 and T19_7 , T9_5 shows a well defined vibronic structure (i.e., 307, 345 and 419 nm).

In particular, the first absorption peaks (Table 1 and Figure 1a–c, yellow symbols) are in agreement with the observations on which the structural design of spider-like oligothiophenes was based: a) T9_5 , T14_6 and T19_7 show a π -conjugation efficiency equivalent to (when considering $E_g(\lambda)$ values, Figure 1b) or even slightly higher than (when considering E_g^* , Figure 1c) linear oligothiophenes having the same number of α -linked thiophene units (i.e., T_5 , T_6 and T_7). b) The energy gap values progressively decrease as n increases up to the critical value of 8–9, then the trend flattens for higher n values (Figure 1c); c) the energy gap values flatten when five α -conjugated thiophene units are present, independently on the whole number of thiophene units constituting the molecule (Figure 1b and c). Indeed, the three TX_n display nearly identical $E_g(\lambda)$ and very similar $E_g^*(\lambda)$ values, independently on the length of the main α -conjugated sequence ($n_\alpha=5, 6, 7$) and on the overall number of thiophene units constituting the molecule ($n=9, 14, 19$), which is more than doubled on passing from T9_5 to T19_7 . This is explained by considering that an increased number of α - α linkages is associated to some distortion from coplanarity, as suggested by the theoretical calculations performed on T14_6 .

On the other hand, the band occurring at about 345 nm could be assigned to absorptions involving the spider legs, as suggested by the extinction coefficient values ϵ (24500 for T9_5 , 52500 for T14_6 and 68700 for T19_7 , Table 1) which are lin-

early dependent on the number of bithienyl pendants present in the molecule (2, 4 and 6). The extinction coefficient is known to be dependent upon the number of the thiophene units also in linear α -oligothiophenes (12500 for T_2 , 26600 for T_4 and 59700 for T_8).^[18]

For T9_5 the lowest 25 TDDFT excitation energies were calculated to provide a detailed assignment of the absorption spectrum. The lowest calculated singlet excited state of T9_5 is a single, very intense, HOMO \rightarrow LUMO excitation which is found at 480 (464) nm ($E_g(\lambda)$, calcd: 2.58 (2.67) eV) using the B3LYP (PBE0) functional. A slightly better agreement with the experimental absorption maximum is computed with the PBE0 functional compared to B3LYP, the former providing a value about 0.3 eV red-shifted compared with the low-energy experimental absorption maximum ($E_g(\lambda)=2.96$ eV). This red-shift is probably due to the extended conjugation of the orbitals involved in this transition, which is not properly captured by DFT-TDDFT but partially corrected by the increased amount of Hartree-Fock exchange present in the PBE0 functional. Notice, that the HOMO–LUMO gap calculated on the basis of the Kohn-Sham orbital energy differences amounts to 2.82 (3.12) eV with the B3LYP (PBE0) functional, so that the slight blue-shift of the lowest absorption band calculated with PBE0 is directly related to the increased HOMO–LUMO gap. The results are reported in Table 2 for the most relevant transitions, together with the experimental absorption data for a direct comparison.

Given the nature of the HOMO and the LUMO discussed above, the lowest energy transition is readily assigned to a π - π^* excitation within the body framework. The band experimentally found at 345 nm appears to be related to two transitions of different character, calculated at 364 and 322 nm, involving both the body and legs framework (Table 2). The band experimentally found at 307 nm is finally calculated to be due to two almost overlapping transitions calculated at 309 and 308 nm; the most intense transition at 308 nm takes place within the legs framework. The calculated vertical transitions are in fair agreement with the experiments; in particular the involvement in the lowest absorption band of the α -conjugated backbone is consistent with the experimental observation that this band is less affected

Table 2. Energy, oscillator strength and composition in terms of molecular orbital excitation of the most relevant vertical transitions calculated with B3LYP (PBE0 data for the lowest transition in parenthesis) for T9_5 , compared to experimental data.

Transition	λ_{max} [nm]	$E_g(\lambda)$ [eV]	Osc. strength	Character
S1	480 (464)	2.58 (2.67)	1.39 (1.44)	HOMO \rightarrow LUMO
S7	364	3.41	0.19	HOMO–3/HOMO \rightarrow LUMO/LUMO+3
S11	322	3.85	0.24	HOMO–2/HOMO–1 \rightarrow LUMO+1/LUMO+2/LUMO+3
S16	309	4.01	0.23	HOMO–3 \rightarrow LUMO+3
S17	308	4.02	0.62	HOMO–2/HOMO–1 \rightarrow LUMO+1/LUMO+2

by increasing the number of spider legs than the higher energy second feature. On the other hand, the fact that the second absorption peak takes place within the spider legs is consistent with the experimental increased intensity of this feature with increasing the number of legs.

TDDFT calculations performed on the two **T14₆** conformers revealed a pattern of vertical excitations similar to that calculated for **T9₅**. In particular, we calculated the lowest excited state to correspond to an intense HOMO–LUMO transition in both cases, but while for the twisted conformer this transition is calculated at 2.55 (2.62) eV with B3LYP (PBE0), similar to the lowest transition in **T9₅**, for the planar conformer a red-shift of the lowest excitation energies is calculated, which brings its value to 2.39 eV at the B3LYP level of theory. This result is consistent with the increased conjugation of the planar conformer. While both results are red-shifted compared with the experiment, the fact that for the most stable twisted conformation we calculate a lowest transition at essentially the same energy as that of **T9₅**, suggests that the twisted conformer dominates the absorption spectrum.

Figure 5 shows that solution PL emission of **T14₆** is red-shifted with respect to that of **T9₅** (emission maximum at about 569 and 524 nm, respectively). This behavior can be explained, if we assume that the lowest excited state geometry corresponds to a planarized structure (see below). This structural rearrangement would induce a stabilization in emission energy due to a more delocalized electronic excitation. In addition it is also possible that energy transfer from branches with shorter conjugation length to branches with more extended conjugation takes place, as observed in dendrimer-like molecules.^[19] Indeed the energetic position of the PL spectra in Figure 5 can be correlated to the increasing degree of molecular branching in **T9₅** and **T14₆**. It is likely that both effects (planarized excited state geometry and intramolecular energy transfer) contribute to observed spectral behavior.

The increased conjugation of the emitting excited states in **T14₆** is supported also by our theoretical investigation, which shows a 0.19 eV red-shift of the lowest excitation energy at the B3LYP level in going from **T9₅** to the planar

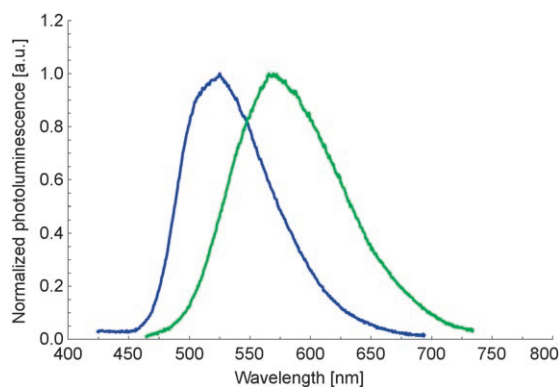


Figure 5. Normalized photoluminescence spectra of **T9₅** (blue) and **T14₆** (green) in CH_2Cl_2 .

T14₆ conformer, as opposed to the more stable twisted **T14₆** conformer, for which we calculate a negligible red-shift of the lowest excitation energy compared with **T9₅**. The calculated excited state stabilization for the planar **T14₆** conformer nicely compares with the 0.15 eV red-shift experimentally observed in emission.

A broad, unstructured and red-shifted emission spectrum like the one of **T9₅** and **T14₆** could possibly be due to the formation of excimers in solution.^[20] However, the presence of excimers can be ruled out because PL measurements at 10^{-6} M concentration provide the same structureless emission, peak position and FWHM of solutions with 10^{-5} M concentration. Moreover, we mention that PL decays are best fitted with a monoexponential function and PL lifetime is the same for both concentrations, which excludes the presence of molecular aggregates.

Electrochemical characterization of TX_n : The electrochemical activity of **T9₅**, **T14₆** and **T19₇** was studied by cyclic voltammetry (CV) in 2.3×10^{-4} M CH_2Cl_2 solution, with TBAP 0.1 M as supporting electrolyte, on glassy carbon (GC) electrode (Figure 6).

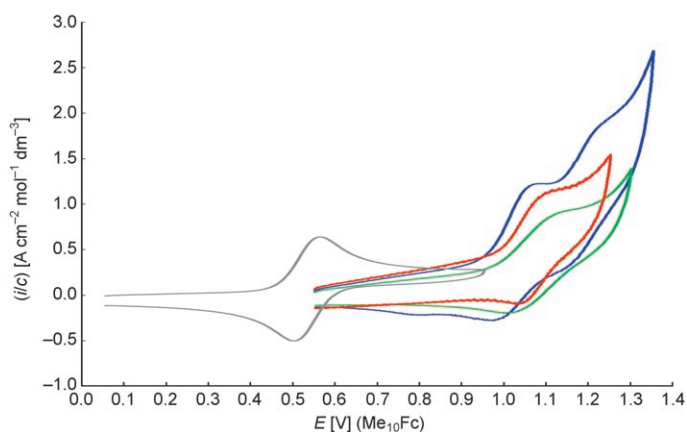


Figure 6. CV patterns of TX_n 0.00023 M in CH_2Cl_2 + TBAP 0.1 M. Color code: blue = **T9₅**, green = **T14₆**, red = **T19₇**. The CV pattern of ferrocene (grey) is also reported for comparison.

As shown by the reversibility parameters $[(E_p - E_{p/2})$ and $(E_{p,i} - E_{p,b})$ Table 3], the first oxidation peaks are electrochemically reversible (mass-transfer controlled reaction with no activation barrier) in the case of **T9₅** and **T19₇**, while **T14₆** tends to partially lose its electrochemical reversibility (i.e., the reaction tends to be kinetically controlled by the electron transfer step), with concomitant shift of the oxidation potential to higher values. This feature points^[5,20] to **T14₆** being more hindered than its lower and higher counterparts in the structural rearrangement required for the first electron extraction (and the concurrent inclusion of either the counter anion or/and solvent molecules), maybe on account of specific conformations pivoted by molecular symmetry, as suggested by calculations which account for a preferred twisted structure of **T14₆**.

Table 3. Voltammetric characterization of TX_n .^[a]

TX_n	$E_{p,A}$ [V]	$E_{p,C}$ [V]	$E_{g,EC}$ [eV]	$E_{p,A}^*$ [V]	$E_{p,C}^*$ [V]	$E_g^*_{EC}$ [eV]
T9 ₅	1.065	-1.652	2.72	0.95	-1.37	2.32
T14 ₆	1.129	-1.608	2.74	1.00	-1.44	2.44
T19 ₇	1.099	-1.728	2.83	0.98	^[b]	^[b]
TX_n	$(E_p - E_{p/2})_A$ [V]	$(E_{p,f} - E_{p,b})$ [V]	$10^5 \times D$ [cm ² s ⁻¹]	$10^5 \times D'$ [cm ² s ⁻¹]		
T9 ₅	0.058	0.076	4.39	4.43		
T14 ₆	0.085	0.110	3.06			
T19 ₇	0.060	0.056	2.19	2.30		

[a] First oxidation and reduction peak potentials ($E_{p,A}$ and $E_{p,C}$, respectively, vs the $\text{Me}_{10}\text{Fc}^+|\text{Me}_{10}\text{Fc}$ redox couple). Onset potentials of first oxidation and reduction peaks, $E_{p,A}^*$ and $E_{p,C}^*$; reversibility parameters for the first oxidation peak (half-peak width, $E_p - E_{p/2}$, and distance between forward and backward peak, $E_{p,f} - E_{p,b}$); band gap energies ($E_{g,EC}$); onset band gap energies ($E_g^*_{EC}$); diffusion coefficients calculated by convolutive analysis (D) and from peak currents (D'). [b] Difficult to obtain.

From the difference between the anodic and cathodic peak potentials it is possible to calculate electrochemical HOMO–LUMO energy gaps $E_{g,EC}$ ^[5,21,22] to be compared with the spectroscopic ones, $E_g(\lambda)$ (Table 1 and Figure 1a–c). To achieve a more complete comparison, “onset” energy gaps, $E_g^*_{EC}$, can be measured also in the electrochemical case (from the difference between the onsets of the first oxidation and reduction peaks) and compared with the absorption ones, $E_g^*(\lambda)$.

It is worthwhile noticing that, although the onset criterion should be regarded as by far less meaningful and more “practical” with respect to the peak-maximum criterion, in this case it appears to lead to better convergence between the two approaches. On the other hand, concerning the alternative criterion based on peak maxima and resulting in a small but significant difference between $E_{g,EC}$ and $E_g(\lambda)$, one must consider that a) the most appropriate comparison with spectroscopic data should require formal potentials E^0 accounting for electrochemically reversible electron transfer processes; unfortunately, in this case, the cathodic process is electrochemically irreversible; b) in any case, the involved energy levels *can* be different in the two approaches since, in the electrochemical case, electrons are subtracted or added to the molecule leading to net charged species (requiring, amongst other things, to take into proper account the possible formation of ionic couples with counter ions from the supporting electrolyte, an effect promoting the electron transfer).

In any case, electrochemical energy gaps of TX_n fully comply, like the spectroscopic ones, with the normalization criteria outlined in the Introduction, based on $E_g(\lambda)$ versus $1/n_\alpha$ plots.

The diffusion coefficients, calculated^[23] either from convolutive analysis of the oxidation peak (D) or from the slope of the current vs. the square root of the potential scan rate straight line (D'), are in good agreement comparing the two methods and show a regular de-

crease (as expected) with the increasing bulkiness of the compounds.

Electrosynthesis of $[\text{TX}_n]_m$ from TX_n and electrochemical characterization of conducting films: Repeated cycling around the first oxidation peak resulted in the formation of conducting films $[\text{TX}_n]_m$. In particular, $[\text{T9}_5]_m$ and $[\text{T14}_6]_m$ show good mechanical properties and are very stable even in the neutral state and after one-month exposure to air. The former is de-

posited with higher efficiency, resulting in a thicker film (confirmed by EQCM). After the electrodeposition cycles, $[\text{T9}_5]_m$ and $[\text{T14}_6]_m$ were characterized in a monomer-free solution (Figure 7 and Table 4). According to MALDI-TOF spectra, $[\text{T9}_5]_m$ is consisting of dimers ($m=2$) and minor amounts of tetramers ($m=4$), while $[\text{T14}_6]_m$ chiefly by dimers.

Both conducting films $[\text{T9}_5]_m$ and $[\text{T14}_6]_m$ show the phenomenon of charge trapping (Figure 8). In fact, the sharp reduction peak associated with the first electron uptake and the concurrent inclusion of the charge-balancing $(\text{C}_4\text{H}_9)_4\text{N}^+$ counter-ion (and possibly also of solvent molecules), presents its oxidative counterpart (associated with the release of the same charge, being characteristically of the same area)

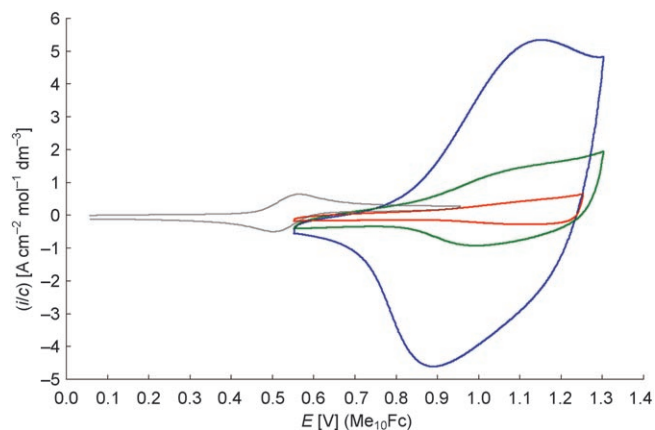


Figure 7. Oxidative CV patterns of $[\text{TX}_n]_m$ after 24 cycles in a monomer free solution. Color code: blue = $[\text{T9}_5]_m$, green = $[\text{T14}_6]_m$, red = $[\text{T19}_7]_m$. The CV pattern of ferrocene (grey) is also reported for comparison.

Table 4. Voltammetric characterization of the electrosynthesized conducting films $[\text{TX}_n]_m$.^[a]

Films	$E_{p,A}$ [V]	$E_{p,C}$ [V]	$E_{g,EC}$ [eV]	$E_{p,A}^*$ [V]	$E_{p,C}^*$ [V]	$E_g^*_{EC}$ [eV]	$E_{A,trap}$ [V]	ΔE_{trap} [eV]
[T9₅]_m	1.16	-1.374	2.54	0.78	-1.25	2.03	0.416	1.79
[T14₆]_m	1.09	-1.378	2.47	0.84	-1.32	2.16	0.590	1.97

[a] First oxidation and reduction potentials (E_A and E_C , respectively, vs the $\text{Me}_{10}\text{Fc}^+|\text{Me}_{10}\text{Fc}$ redox couple); energy band gaps ($E_{g,EC}$); oxidation potential corresponding to the recovery of the trapped charge $E_{A,trap}$ and charge-trapping energy (ΔE_{trap}).

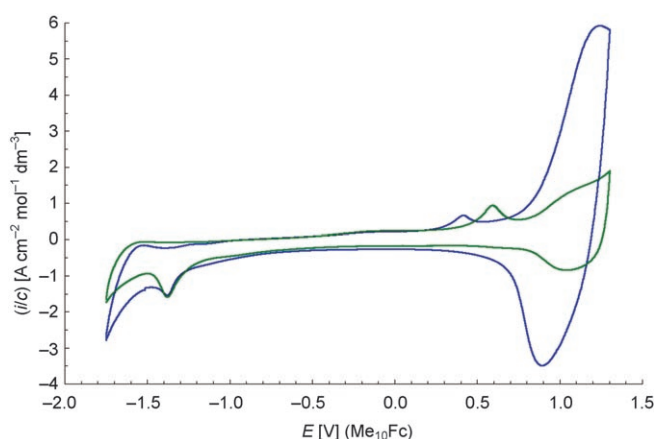


Figure 8. Complete CV patterns of $[\text{TX}_n]_m$ in the monomer free solution. Color code: blue = $[\text{T9}_5]_m$, green = $[\text{T14}_6]_m$.

only at very positive potentials, just before the first “regular” oxidation peak, corresponding to the radical cation formation.

The large charge-trapping potential difference (no less than 1.8–2.0 V, see ΔE_{trap} in Table 4), related to a significant free energy change, could be associated to a significant structural reorganization step with conjugative redistribution of the negative charge. It is probable that the delocalization of the injected charge on the wide π -system network, having many freedom degrees (particularly in the secondary branches) together with the concurrent inclusion of counter cations (and possibly solvent molecules), prompts a transition to a more favourable and stabilized structure, involving significant intra- and/or supramolecular reorganization. Accordingly, a more positive potential is required to release the charge since an extra energy contribution is required to recover the original structure. In particular, while the injection of the negative charge occurs at the same potential for the two materials, the potential required to release the charge in the case of $[\text{T14}_6]_m$ is significantly more positive. This could be connected to its larger and more branched structure, resulting in more complex reorganization requirements to accommodate the incoming charge and the corresponding counter-ion.

In situ conductivity experiments were performed only for $[\text{T9}_5]_m$, because $[\text{T14}_6]_m$ failed to bridge the two-band electrode^[24] or underwent dissolution during analysis.

Conductivities of $[\text{T9}_5]_m$ are quite satisfactory, showing a linear dependency on the potential, ranging from 0.1 Scm^{-1} at 0.85 V (Me_{10}Fc) to the promising value of 6.5 Scm^{-1} at 1.25 V (Me_{10}Fc).

Spectroscopic properties of $[\text{TX}_n]_m$: The UV absorption data of $[\text{TX}_n]_m$ are reported in Figure 9a and summarized in Table 4. The UV/Vis absorption spectra of $[\text{T9}_5]_m$ and $[\text{T14}_6]_m$ films shift to significantly longer wavelengths with respect to the corresponding TX_n , thus confirming that coupling has indeed occurred resulting in a more extended π -conjugated system (Table 5 and Figure 9). This conjugation

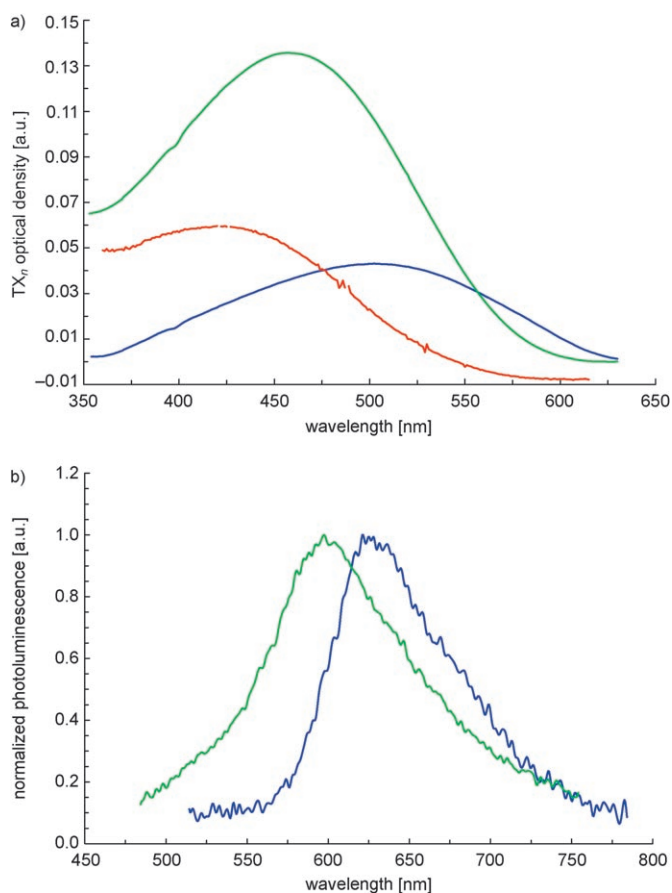


Figure 9. a) UV/Vis spectra of $[\text{TX}_n]_m$ on ITO. b) Photoluminescence spectra of $[\text{T9}_5]_m$ and $[\text{T14}_6]_m$ on ITO. Color code: blue = $[\text{T9}_5]_m$, green = $[\text{T14}_6]_m$, red = $[\text{T19}_7]_m$.

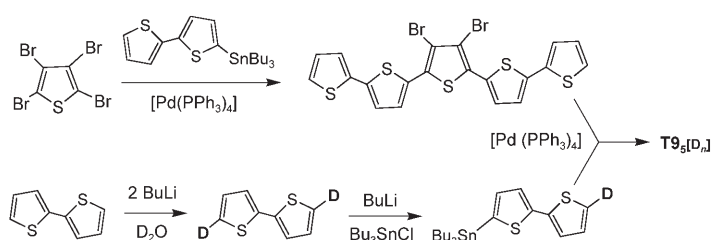
Table 5. UV characterization of the electrosynthesized conducting films $[\text{TX}_n]_m$.

Films	λ_{max} [nm]	$E_g(\lambda)$ [eV]	λ_{onset} [nm]	$E_g^*(\lambda)$ [eV]
$[\text{T9}_5]_m$	502	2.47	630	1.97
$[\text{T14}_6]_m$	456	2.72	610	2.03
$[\text{T19}_7]_m$	424	2.93	575	2.16

improvement is significantly higher than the expected one considering oligomers in solution (Figure 1b and c); this points to a solid-state effect, possibly connected with π -stack interactions between adjacent molecules at short inter-chain distances in the conducting film.^[25] Experiments reveal that $[\text{T9}_5]_m$ has the onset of the optical absorption at the longest wavelength (i.e., it has the more extended conjugation), while $[\text{T19}_7]_m$ has the shortest conjugation. These findings can be interpreted considering that $[\text{T9}_5]_m$ has the highest α - α constitutional order (see below) and then a higher conjugation degree. The regular increase of the α'/α position ratio in the $[\text{TX}_n]_m$ series (from 1 to 3) necessarily results in a decrease of the α - α coupling regioselectivity, implying shorter α -conjugated chains in the films. Consistently with absorption, the photoluminescence spectra of $[\text{T9}_5]_m$

and $[T14_6]_m$ (Figure 9b) are at lower energy with respect to the ones of the corresponding monomers, confirming the longer effective π conjugation in the films. The maximum emission wavelengths of $[T9_5]_m$ and $[T14_6]_m$ are located at about 630 and 610 nm, respectively, again suggesting a more extended conjugation in $[T9_5]_m$ with respect to $[T14_6]_m$.

Investigation of the regiochemistry of the electrochemical oxidative coupling of $T9_5$: The polymerization of monomers, where heterotopic thiophene moieties with free α positions are present, opens the question which rings are involved in the oxidative coupling process. To answer this question we resorted to labelled monomer $T9_5[D_n]$ ($n=0, 1, 2$) in which both α positions of the branches are labelled with deuterium (Scheme 3). By computing the isotopic abundance in the



Scheme 3. Synthesis of labelled $T9_5[D_n]$.

electrooxidation products and in the starting monomer at different times it was possible to evaluate the relative kinetic parameters for the coupling reaction between two α positions (Scheme 2) of the fully 2,5-conjugated system (α - α coupling), between two α' positions of thiophene rings belonging to the branches (α' - α' coupling), and for the mixed coupling α - α' coupling).

Labelled $T9_5[D_n]$ was prepared according to the reaction sequence reported in Scheme 3, taking advantage of the higher reactivity of the bromine atoms in position α of tetrabromothiophene.^[3]

Laser-desorption-ionization (LDI) mass spectrometric analysis gave the isotopic distribution in the starting $T9_5[D_n]$ monomer shown in Table 6. The regioselectivity of the labelling was proven by the nearly total absence in the 1H NMR spectrum of a signal (dd) at δ 7.17 ppm, due to the α' hydrogens of $T9_5$.

Electrooxidative coupling of $T9_5[D_n]$, carried out under the experimental conditions described before for $T9_5$, afforded the expected mixture of dimer $D[D_x]$ and tetramer, where $D[D_x]$ ($x=0-4$) refers to the unlabelled, mono-, bis-, tris- and tetradeuterated dimer. The analysis of the peak abundance in the LDI spectrum of dimer $D[D_x]$, obtained after an about 2% conversion, revealed the isotopic distribution reported in Table 6.

The 8.5% abundance of unlabelled dimer $D[D_0]$ is not compatible with the very modest presence of unlabelled $T9_5[D_0]$ in the starting material (2%).

This hints that some deuterium is lost during the electrooxidation. To check this hypothesis, a sample of monomer

Table 6. Deuterium distribution [%] in the monomer $T9_5[D_n]$ and in the dimer $D[D_x]$ resulting from its electrooxidation at different conversion levels.

$T9_5[D_n]$ conv = 0%	$T9_5[D_0]$	$T9_5[D_1]$	$T9_5[D_2]$		
	2	10	88		
$T9_5[D_n]$ conv = 64%	$T9_5[D_0]$	$T9_5[D_1]$	$T9_5[D_2]$		
	17	16	67		
$D[D_x]$ conv = 2%	$D[D_0]$	$D[D_1]$	$D[D_2]$	$D[D_3]$	$D[D_4]$
	8.5	9.5	17	22	43

$T9_5[D_n]$ was recovered after that the oxidation was driven to 64% conversion. The isotopic abundance in recovered $T9_5[D_n]$ (Table 6) confirmed that significant H-D exchange occurred during the oxidative process.

To explain such D-H exchange phenomenon in the monomer, we suggest a mechanism in which the radical cation resulting from electrooxidation can either react with another radical cation to ultimately give the dimer $D[D_x]$, or exchange deuterium with protium by hydrogen abstraction from an undefined species present in solution.

To obtain an estimate of the regiochemistry of the dimerization, that is, of the relative velocity of the $\alpha\alpha$, $\alpha\alpha'$ and $\alpha'\alpha'$ dimerization reactions, one needs to interpret the deuterium distribution in the dimer by means of a kinetic scheme (see below).



To obtain the five rate constants from experimental data, we followed a best-fit procedure consisting in: 1) integrating the rate laws (1) under mass balance constraint, 2) finding the 2% conversion point, 3) computing the deuterium distribution in the dimer at 2% conversion and comparing it with the experimental one. Using this way, the kinetic constants which best fit to the experimental data within a given kinetic model are obtained. The relative magnitude of the best-fit kinetic constants are reported in Table 7 and the calculated deuterium distribution in the dimer is pictured in Figure 10, either in the absence or in the presence of the deuterium exchange reaction.^[1b]

Table 7. Relative magnitude of the best-fit kinetic constants of the kinetic model (1) with and without the radical cation dedeuteration step (1b).

	Dedeuteration reaction (1b)	
	Present	Absent
k_{dd}/k_{ox}	27	-
$k_{\alpha\alpha}/k_{ox}$	41	0.57
$k_{\alpha\alpha'}/k_{ox}$	0.033	0.12
$k_{\alpha'\alpha'}/k_{ox}$	0	0

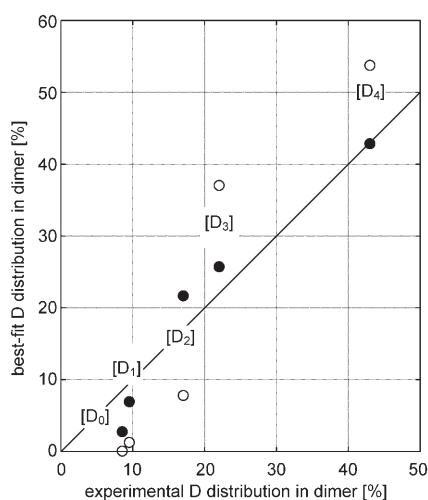


Figure 10. Comparison of the experimental deuterium distribution in dimer and the best-fit distribution. ●: best-fit to the kinetic model including the monomer dedeuteration step;^[1b] ○: best-fit to the kinetic model without monomer dedeuteration.

As it can be seen in Figure 10, the introduction of the deuterium loss in the kinetic model greatly improves the quality of the fit for all dimer deuteration levels. The small differences between the experimental and best-fit distribution are not much larger than the experimental error. Hence, this simple kinetic analysis indicates that deuterium loss from the monomer is able to explain the observed deuterium levels in the dimer. The dimerization turns out to be a very regioselective reaction. The $\alpha\alpha$ coupling is more than 1000 times faster than the $\alpha\alpha'$ coupling and the $\alpha'\alpha'$ dimerization is practically absent. It is also interesting that the dedeuteration kinetic constant is of the same order of magnitude as $k_{\alpha\alpha}$.

Conclusion

T9₅, **T14₆** and **T19₇** open a class of all-thiophene-based materials tailored to couple good performances, and synthetic accessibility. They have been designed on the basis of a careful investigation of the optical properties–structure relationships in molecules described in recent literature. **T9₅** and **T14₆** have been prepared on a multi-gram scale in good yields starting from inexpensive, commercially available materials. They feature first oxidation CV peaks of reversible or quasi-reversible character, affording fast and reproducible formation of conducting [**TX_n**]_m films. The films, mainly consisting of dimers, are highly stable and show a significant increase in π delocalization together with an impressive charge-trapping ability, probably connected with molecular and supramolecular reorganization related to the many freedom degrees of the branched structure. [**T9₅**]_m, which has been demonstrated to possess a high α - α constitutional order, displays the smallest optical gap, indicating that the formation of films from larger members involves distortion

or lower constitutional order. Photoluminescence spectroscopy reveals that larger sized **TX_n** are red-shifted with respect to smaller ones and that [**T9₅**]_m has the lower emission energy. This result is interpreted in terms of a trade-off between the length of α -linked chains and conjugation interruptive distortions. DFT-TDDFT calculations allowed us to gain insight into the structural, electronic and optical properties of the investigated systems, providing a detailed assignment of the absorption spectrum of **T9₅** and of **T14₆**. At variance with **T9₅**, for which the ground state is clearly planar, for **T14₆** we found two almost isoenergetic minima corresponding to a planar and a twisted structure. The calculated absorption spectrum of the more stable **T14₆** twisted conformer is consistent with the experimental trend of absorption, while the red-shift of the lowest transition calculated for **T14₆** planar conformer is suggestive of a planar geometry for the emitting excited state.

Spider-like oligothiophenes are promising materials for applications as active layers in multifunctional organic devices,^[20] where fine tuning between charge transport ability, intermolecular interactions and light emission efficiency is crucial.

Experimental Section

Organic synthesis: NMR spectra were obtained on Bruker AV 400 and Bruker AC 300 spectrometers. Chemical shifts were recorded in ppm and the coupling constants were reported in Hz. Mass spectra were recorded on Bruker Daltonics high resolution FT-ICR (Fourier Transform Ion Cyclotron Resonance) model APEXIM II (4.7 Tesla Magnex cryomagnet supplied with ESI source) and ThermoFinnigan LCQ Advance (ESI and APCI sources). MALDI spectra were recorded on a Bruker Microflex LT spectrometer. DSC curves were recorded on a Mettler DSC 823. THF was freshly distilled from sodium/benzophenone. All reagents were commercially available and were used as received. The normal work-up included extraction, drying over Na₂SO₄ and evaporation of volatile materials in vacuo. Purifications by column chromatography were performed using Merck silica gel 60 (230–400 mesh for flash chromatography and 70–230 mesh for gravimetric chromatography). NMR and MS spectra are given in the Supporting Information.

Bis[3',4'-(5,2'-bithiophen-2-yl)]-2,2':5',2''':5''':2''''-pentathiophene (T9₅): 5-Tributylstannyl-2,2'-bithiophene (2.5 g, 5.49 mmol) and [Pd(PPh₃)₄] (101 mg, 0.0874 mmol) were added under nitrogen atmosphere to a stirred solution of tetrabromothiophene (350 mg, 0.876 mmol) in toluene (10 mL). The mixture was heated under reflux for 18 h and filtered on silica gel to remove the catalyst residue. Toluene was evaporated under reduced pressure and the residue was triturated with hexane (3 × 15 mL) to remove organotin in excess and tin side products. Purification by flash chromatography (silica gel, hexane/chloroform 7:3) yielded **T9₅** (585 mg, 90%) as a yellow-orange solid. M.p. (DSC) 215 °C; ¹H NMR (300 MHz, CDCl₃): δ = 7.17 (m, 2H), 7.11 (dd, 2H, J_1 = 4.7, J_2 = 1.2 Hz), 7.09 (dd, 2H, J_1 = 3.6, J_2 = 1.1 Hz), 7.06 (d, 2H, J = 3.7 Hz), 7.02 (brs, 4H), 6.97 (d, 2H, J = 3.6 Hz), 6.96 (d, 2H, J = 3.6 Hz), 6.86 ppm (d, 2H, J = 3.7 Hz); ¹³C NMR (300 MHz, CDCl₃): δ = 139.41, 138.36, 137.33, 136.9, 134.08, 133.9, 133.48, 132, 130.35, 127.84, 127.74, 127.18, 124.71, 124.33, 124.03, 123.81, 123.62 ppm; MS (EI): m/z : 740 (100) [M]⁺; HRMS: m/z calcd for C₃₆S₉H₂₀⁺: 739.90515; found: 739.90558.

Tetrakis[3',4',3''',4''''-(5,2'-bithiophen-2-yl)]-2,2':5',2''':5''':2''''-hexathiophene (T14₆): 5-Tributylstannyl-2,2'-bithiophene (2.87 g, 6.312 mmol) and [Pd(PPh₃)₄] (182 mg, 0.157 mmol) were added under nitrogen atmosphere to a stirred solution of hexabromo-2,2'-bithiophene (0.5 g, 0.789 mmol) in xylene (25 mL). The mixture was heated under

state 10 W CW laser. The fundamental emission of the Ti/sapphire laser is coupled into a β -barium borate (BBO) crystal for second harmonic generation before exciting sample photoluminescence at a wavelength of 400 nm. PL spectra were then measured using a Chromex monochromator with spectral resolution of 2 meV.

LDI spectrometry: Laser desorption-ionization (LDI) mass spectra were obtained by an ULTRAFLEX II (Bruker Daltonics, Bremen, Germany) instrument. 1 μ L of oligothiophenes solution (5 μ g mL⁻¹ in CHCl₃) was deposited on the MALDI plate. After sample drying, the LDI spectra were acquired with ion source 1 (IS1) set to 25 kV, ion source 2 (IS2) set to 21.65 kV, lens voltage set to 10.5 kV and with a delay extraction of 0 sec. The laser (N₂, 337 nm) energy employed was 81.2 μ J (70% of its maximum value). Dithranol was used as the matrix for the MALDI spectra.

Acknowledgements

Work supported by MIUR: FIRB-RBNE033KMA "Composti molecolari e materiali ibridi nanostrutturati con proprietà ottiche risonanti e non risonanti per dispositivi fotonici" and PRIN; by EU Commission: FP6-015034 (OLAS) and FP6 035859 (BIMORE). T.B. thanks the Dipartimento di Chimica Organica e Industriale of the University of Milan for the hospitality.

- [1] A. Bilge, A. Zen, M. Forster, H. Li, F. Galbrecht, B. S. Nehls, T. Farrell, D. Neher, U. Scherf, *J. Mater. Chem.* **2006**, *16*, 3177.
- [2] a) Y. Nicolas, P. Blanchard, E. Levillain, M. Allain, N. Mercier, J. Roncali, *Org. Lett.* **2004**, *6*, 273.
- [3] B. X. Sun, Y. Liu, S. Chen, W. Qiu, G. Yu, Y. Ma, T. Qi, H. Zhang, X. Xu, D. Zhu, *Adv. Funct. Mater.* **2006**, *16*, 917.
- [4] C. Ma, E. Mena-Osteriz, T. Debaerdemaeker, M. M. Wienk, R. A. J. Janssen, P. Bauerle, *Angew. Chem.* **2007**, *119*, 1709; *Angew. Chem. Int. Ed.* **2007**, *46*, 1679.
- [5] a) C. Xia, X. Fan, J. Locklin, R. C. Advincula, *Org. Lett.* **2002**, *4*, 2067; b) C. Xia, X. Fan, J. Locklin, R. C. Advincula, A. Gies, W. Nonidez, *J. Am. Chem. Soc.* **2004**, *126*, 8735; c) R. C. Advincula, *Dalton Trans.* **2006**, 2778.
- [6] K. Meerholz, J. Heinze, *Electrochim. Acta* **1996**, *41*, 1839.
- [7] a) N. Negishi, Y. Ie, M. Taniguchi, T. Kawai, H. Tada, T. Kaneda, Y. Aso, *Org. Lett.* **2007**, *9*, 829; b) W. J. Mitchell, N. Kopidakis, G. Rumbles, D. S. Ginley, S. E. Shaheen, *J. Mater. Chem.* **2005**, *15*, 4518; c) S. A. Ponomarenko, S. Kirchmeyer, A. Elschner, B.-H. Huisman, A. Karbach, D. Drechsler, *Adv. Funct. Mater.* **2003**, *13*, 591.
- [8] J. Nakayama, K. Sawada, A. Ishii, M. Hoshino, *Heterocycles* **1992**, *34*, 1487.
- [9] G. Tour, R. Wu, *Macromolecules* **1992**, *25*, 1901.
- [10] G. Barbarella, L. Favaretto, G. Sotgiu, M. Zambianchi, V. Fattori, M. Cocchi, F. Cacialli, G. Gigli, R. Cingolati, *Adv. Mater.* **1999**, *11*, 1379.
- [11] K. Yui, Y. Aso, T. Otsubo, F. Ogura, *Bull. Chem. Soc. Jpn.* **1989**, *62*, 1539.
- [12] W. Steinkopf, R. Leitsmann, K. Hofmann, *Ann.* **1941**, *546*, 180.
- [13] A. D. Becke, *J. Chem. Phys.* **1993**, *98*, 5648.
- [14] J. S. Binkley, J. A. Pople, and W. J. Hehre, *J. Am. Chem. Soc.* **1980**, *102*, 939.
- [15] J. P. Perdew, K. Burke, M. Ernzerhof, *Phys. Rev. Lett.* **1996**, *77*, 3865.
- [16] C. Adamo, G. E. Scuseria, V. Barone, *J. Chem. Phys.* **1999**, *111*, 2889.
- [17] Gaussian 03, Revision D01, M. J. Frisch, G. W. Trucks, H. B. Schlegel, G. E. Scuseria, M. A. Robb, J. R. Cheeseman, J. A. Montgomery, Jr., T. Vreven, K. N. Kudin, J. C. Burant, J. M. Millam, S. S. Iyengar, J. Tomasi, V. Barone, B. Mennucci, M. Cossi, G. Scalmani, N. Rega, G. A. Petersson, H. Nakatsuji, M. Hada, M. Ehara, K. Toyota, R. Fukuda, J. Hasegawa, M. Ishida, T. Nakajima, Y. Honda, O. Kitao, H. Nakai, M. Klene, X. Li, J. E. Knox, H. P. Hratchian, J. B. Cross, C. Adamo, J. Jaramillo, R. Gomperts, R. E. Stratmann, O. Yazyev, A. J. Austin, R. Cammi, C. Pomelli, J. W. Ochterski, P. Y. Ayala, K. Morokuma, G. A. Voth, P. Salvador, J. J. Dannenberg, V. G. Zakrzewski, S. Dapprich, A. D. Daniels, M. C. Strain, O. Farkas, D. K. Malick, A. D. Rabuck, K. Raghavachari, J. B. Foresman, J. V. Ortiz, Q. Cui, A. G. Baboul, S. Clifford, J. Gaussian, Inc., Pittsburgh PA, **2003**.
- [18] Handbook of Oligo- and Polythiophenes (Ed.: D. Fichou), Wiley-VCH, Weinheim, **1999**; P. Bäuerle, T. Fischer, B. Bidlingmeier, A. Stabel, J. P. Rabe, *Angew. Chem.* **1995**, *107*, 335; *Angew. Chem. Int. Ed. Engl.* **1995**, *34*, 303.
- [19] O. Varnasky, *J. Chem. Phys.* **2002**, *116*, 8893.
- [20] M. Muccini, *Nature Mater.* **2006**, *5*, 605.
- [21] P. Dandliker, F. Diederich, M. Gross, C. Knobler, A. Louati, E. Sanford, *Angew. Chem.* **1994**, *106*, 1821; *Angew. Chem. Int. Ed. Engl.* **1994**, *33*, 1739.
- [22] a) M. Catellani, C. Arbizzani, M. Mastragostino, A. Zanelli, *Synth. Met.* **1995**, *69*, 373; b) Z. Peng, Y. Pan, B. Xu, J. Zhang, *J. Am. Chem. Soc.* **2000**, *122*, 6619; c) M. Mastragostino, C. Arbizzani, A. Bongini, G. Barbarella, M. Zambianchi, *Electrochim. Acta* **1993**, *38*, 135; d) K. Faid, R. Cloutier, M. Leclerc, *Macromolecules* **1993**, *26*, 2501; e) L. E. Bolivar-Marinez, M. C. dos Santos, D. S. Galvão, *J. Phys. Chem.* **1996**, *100*, 11029.
- [23] A. J. Bard, L. R. Faulkner, *Electrochemical Methods*, Wiley-VCH, New York, USA, **2002**, pp. 247–252.
- [24] G. Schiavon, S. Sitran, G. Zotti, *Synth. Met.* **1989**, *32*, 209.
- [25] M. Muccini, E. Lunedei, C. Taliani, D. Beljonne, J. Cornil, J. L. Brédas, *J. Chem. Phys.* **1998**, *109*, 10513; M. Muccini, E. Lunedei, A. Bree, G. Horowitz, F. Garnier, C. Taliani, *J. Chem. Phys.* **1998**, *108*, 7327.
- [26] A. J. Bard, L. R. Faulkner, *Electrochemical Methods*, Wiley-VCH, New York, USA, **2002**, pp. 648–650.
- [27] a) L. Falciola, A. Gennaro, A. A. Isse, P. R. Mussini, M. Rossi, *J. Electroanal. Chem.* **2006**, *593*, 47; b) J. Ruiz, D. Astruc, *Comptes Rendus Acad. Sci. Série IIc: Chimie* **1998**, *1*, 21; c) I. Noviadri, K. N. Brown, D. S. Fleming, P. T. Gulyas, P. A. Lay, A. F. Masters, L. Phillips, *J. Phys. Chem. A* **1999**, *103*, 6713.
- [28] a) G. Gritzner, J. Kuta, *Pure Appl. Chem.* **1984**, *56*, 461; b) G. Gritzner, *Pure Appl. Chem.* **1990**, *62*, 1839.
- [29] A. J. Bard, L. R. Faulkner, *Electrochemical Methods*, Wiley-VCH New York, USA, **2002**, pp. 228–232.
- [30] A. J. Bard, L. R. Faulkner, *Electrochemical Methods*, Wiley-VCH, New York, USA, **2002**, pp. 247–252.
- [31] G. Tourillon, F. Garnier, *J. Phys. Chem.* **1983**, *87*, 2289.

Received: July 19, 2007
Published online: November 28, 2007